Electronic Supplementary Information (ESI)

Multimetal synergy in iron-cobalt-nickel hydroxide electrocatalyst for electro-oxidative lignin depolymerization to produce value-added aromatic chemicals

Pengfeng Li,[a] Jiaqi Zhang,[a] Shanshan Liu,[b] Fengcai Lei,[a] Xu Sun,[c] Junfeng Xie[a,*]

a *College of Chemistry, Chemical Engineering and Materials Science, Key Laboratory of Molecular and Nano Probes (Ministry of Education), Collaborative Innovation Center of Functionalized Probes for Chemical Imaging in Universities of Shandong, Shandong Normal University, Jinan, Shandong, 250014, P. R. China. E-mail: xiejf@sdnu.edu.cn.*

b College of Chemical Engineering and Safety, Shandong University of Aeronautics, Binzhou, Shandong, 256603, P. R. China.

c *Key Laboratory of Interfacial Reaction & Sensing Analysis in Universities of Shandong, School of Chemistry and Chemical Engineering, University of Jinan, Jinan 250022, Shandong, P. R. China.*

S1. Experimental section

S1.1 Chemicals

The chemicals were purchased from Sinopharm Chemical Reagent Co., Ltd. and used as received without further purification.

S1.2 Material synthesis

The nickel foam (NF)-supported iron-cobalt-nickel hydroxide nanosheet array ($FeCoNi(OH)_x$@NF) was synthesized via a one-step hydrothermal approach. Typically, $Fe(NO_3)_3 \cdot 9H_2O$ (0.2 mmol), $Co(NO_3)_2 \cdot 6H_2O$ (0.2 mmol), $Ni(NO_3)_2 \cdot 6H_2O$ (0.2 mmol), and 1.2 mmol of urea was dissolved in 80 mL of deionized water and stirred for 20 min to form a transparent solution. After that, a piece of nickel foam (4 × 1 cm) was ultrasonically treated in ethanol for 5 min to remove the surface organics, immersed in 1% HCl solution for 5 min to remove the oxide layer on the surface, and washed with deionized water for several times. Then, the nickel foam was placed in a 100 mL Teflon-lined stainless-steel autoclave, and the precursor solution was added. The autoclave was then sealed and maintained at 160 ºC for 12 h, and then allowed to cool to room temperature. The as-obtained products were rinsed with deionized water and absolute ethanol for several times, and dried in a vacuum drying oven at 40 °C for 12 h. For the synthesis of binary $CoNi(OH)_x$@NF, equal amounts of $Co(NO_3)_2 \cdot 6H_2O$ (0.3 mmol), $Ni(NO_3)_2 \cdot 6H_2O$ (0.3 mmol) were used as the precursor, and the other parameters were unchanged. For the synthesis of unary $Co(OH)_2$@NF, 0.6 mmol $Co(NO_3)_2 \cdot 6H_2O$ was used as the precursor, and the other parameters were unchanged.

S1.3 Structural characterizations

The X-ray diffraction (XRD) was performed on a Philips X'Pert Pro Super diffractometer with Cu Kα radiation (λ = 1.54178 Å). The scanning electron microscopy (SEM) images were taken on a JEOL JSM-6700F SEM. The transmission electron microscopy (TEM) was carried out on a JEM-2100F field emission electron microscope at an acceleration voltage of 200 kV. The high-resolution TEM (HRTEM), high-angle annular dark-field scanning transmission electron microscopy (HAADF-STEM) and corresponding elemental mapping analyses were performed on a Thermo Fischer Talos

F200X TEM. The X-ray photoelectron spectroscopy (XPS) analyses were performed on a VGESCALAB MKII X-ray photoelectron spectrometer with an excitation source of Mg Kα = 1253.6 eV, and the resolution level was lower than 1 atom%. The Gas chromatography-mass spectrometry (GC-MS) measurements were conducted on a Shimadzu GCMS-QP2010 plus equipment. The detailed parameters for the tests are listed as following: The electrolyte was extracted with ethyl acetate; Column DB-1MS (30 m × 1 μm × 0.32 mm) (Agilent); temperature rise rate 60 °C~2min~300 °C (temperature rise rate 15 °C/min) held for 20 min, split ratio 20:1, constant linear velocity mode 56.8 cm/s, carrier gas He ion; source temperature 200 °C, interface temperature 300 °C, injection port temperature 320 °C; mass scanning range 29-550 m/z; injection volume 1 μL, the sample was filtered by a disposable syringe with a 0.22 μm organic filter membrane and the library was retrieved from the NIST 2017 standard library. The ^{1}H nuclear magnetic resonance (NMR) spectroscopy was tested on a Bruker AVANCE 400 NMR instrument. The tested sample was a mixture of 500 μL electrolyte and 100 μL D_2O, and maleic acid was selected as the internal standard.

S1.4 Electrocatalytic study

All the electrochemical measurements were performed in a three-electrode system linked with an electrochemical workstation (CHI660E) at room temperature. All potentials were calibrated to a reversible hydrogen electrode (RHE) and the data are presented without iR correction. An Hg/HgO electrode was used as the reference electrode, a platinum gauze electrode (2 × 2 cm, 60 mesh) was used as the counter electrode, and the nanoarray catalyst was served as the working electrode which was fixed with an electrode holder connected by a glassy carbon plate. The linear sweeping voltammetry (LSV) tests were conducted at a scan rate of 2 mV s^{-1}. For the measurement of electro-oxidative lignin depolymerization, 5 mL mixed solution of acetonitrile-water (V_{MeCN}:V_{H2O} = 1:4) with 1 g L^{-1} lignin model (2-phenoxy-1-phenylethanol) and 0.5 M KOH was used as the electrolyte. For OER test, a mixed solution of acetonitrile-water (V_{MeCN}:V_{H2O} = 1:4) with 0.5 M KOH was used. The electrochemical impedance spectroscopy (EIS) measurements were operated at variable potentials from 10^{-2}-10^{5} Hz at 1.5 V vs. RHE. The lignin depolymerization rate can be

described as the conversion rate of lignin model, which is the ratio of depolymerized lignin model per total lignin model. The residual lignin model after the electrocatalytic operation can be quantitatively determined by ^{1}H NMR spectra. Hence, the conversion rate of lignin model can be defined as:

$$\text{Conversion rate (\%)} = (n_{total} - n_{residual}) / n_{total} \times 100\%$$

S2. Supplementary physical and electrochemical characterizations

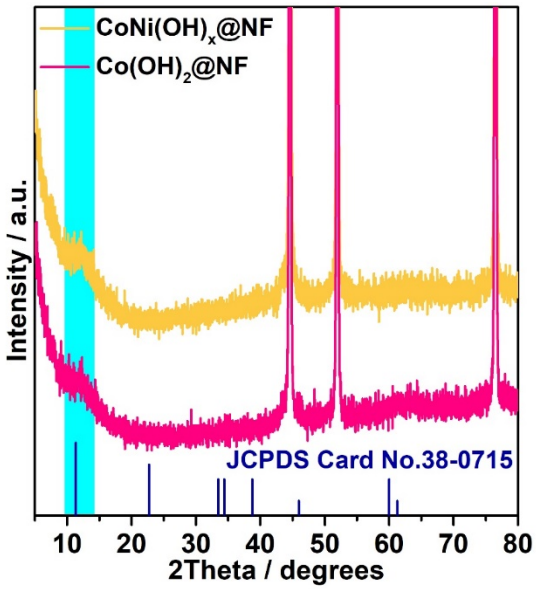

Fig. S1 XRD patterns of the binary $CoNi(OH)_x$@NF and unary $Co(OH)_2$@NF.

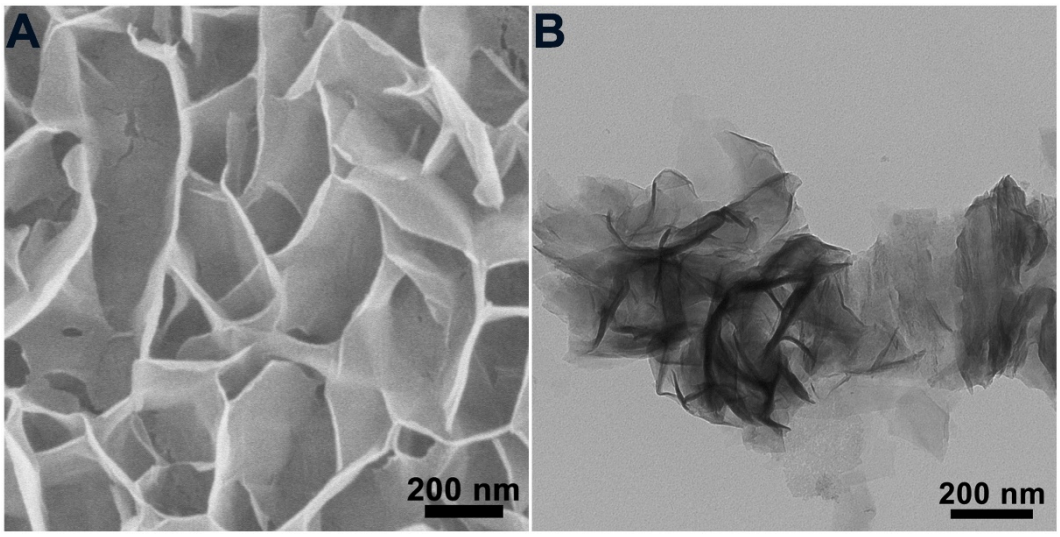

Fig. S2 (A-B) SEM and TEM images of the binary $CoNi(OH)_x$@NF.

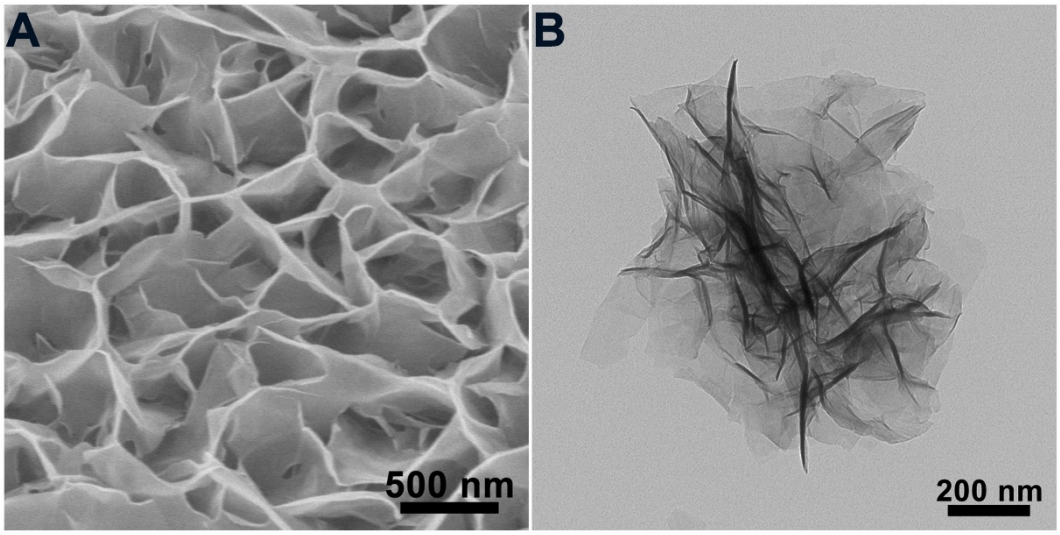

Fig. S3 (A-B) SEM and TEM images of the unary $Co(OH)_2$@NF.

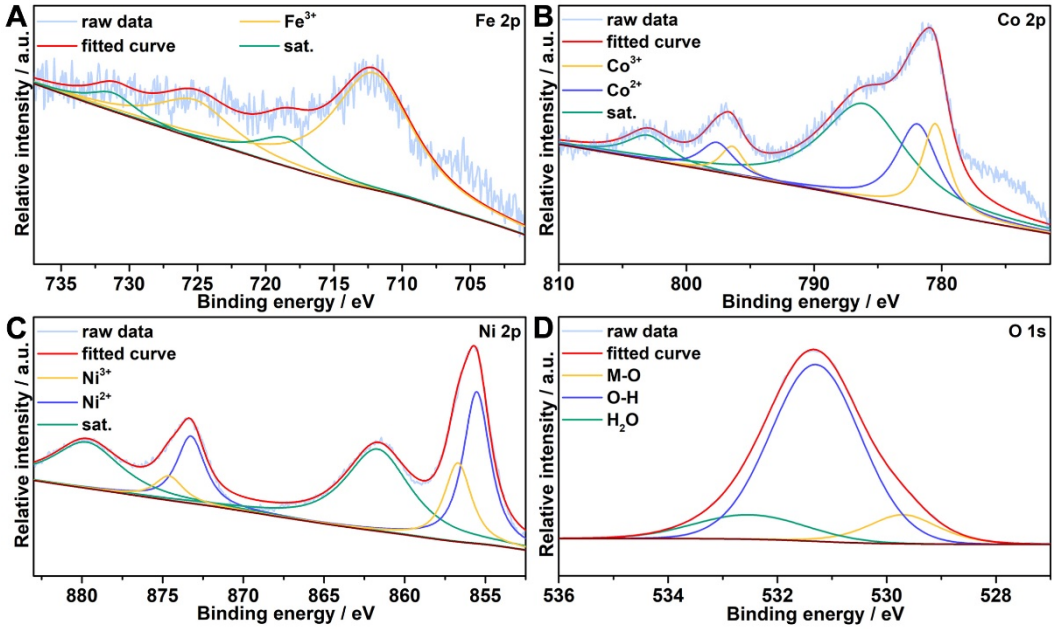

Fig. S4 XPS spectra of the ternary $FeCoNi(OH)_x$@NF catalyst. (A) Fe, (B) Co, (C) Ni, (D) O.

The composition and valence characteristics of the ternary $FeCoNi(OH)_x$@NF catalyst was identified by means of X-ray photoelectron spectroscopy (XPS). As shown in Fig. S4A, Fe 2p spectrum confirms the dominance of Fe^{3+} ions with deconvoluted peaks centered at 712.0 eV and 724.9 eV.[1] The Co 2p spectrum in Fig. S4B reveals two pairs of deconvoluted peaks with binding energies of 781.9/797.6 eV

and 780.5/796.4 eV, which can be assigned to Co^{2+} and Co^{3+} species, respectively.[2] Besides, the Ni 2p spectrum in Fig. S4C can be indexed as Ni^{2+} ions (855.5 and 873.2 eV) and Ni^{3+} ions (856.7 and 874.6 eV).[3] The local high-valence species could effectively act as the active sites for the electro-oxidation reactions. In addition, as shown in Fig. S4D, the O 1s spectrum displays an intensive peak with binding energy of 531.3 eV, corresponding to the hydroxyl group in the hydroxide material. The other two peaks centered at 529.7 eV and 532.5 eV can be assigned to M-O bonding and the adsorbed water.[4]

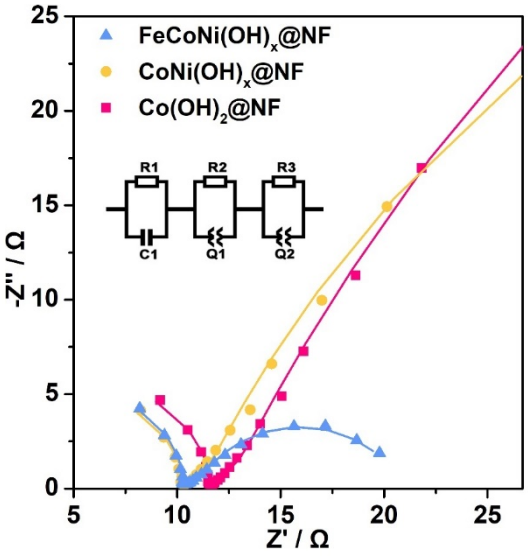

Fig. S5 EIS data of the catalysts.

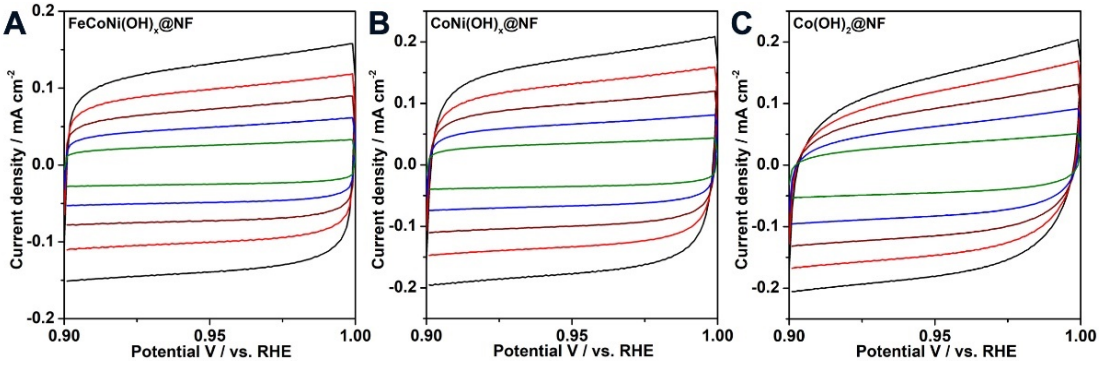

Fig. S6 CV curves of the catalysts measured in a non-redox region for evaluating the C_{dl} values. (A) $FeCoNi(OH)_x$@NF, (B) $CoNi(OH)_x$@NF, (C) $Co(OH)_2$@NF.

The estimation of the effective active surface area was carried out according to literature.[5] Typically, cyclic voltammetry (CV) tests were conducted at various scan rates (20, 40, 60, 80, 100 mV s^{-1}) in the region of 0.9~1.0 V vs. RHE where no redox reaction occurs (Fig. S6), which can be considered as the double-layer capacitive behavior. The electrochemical double-layer capacitance (C_{dl}) was estimated by plotting the Δj (j_a-j_c) at 0.95 V vs. RHE against the scan rates, where the slope is twice C_{dl} (Fig. 2C). The resulted C_{dl} values of the catalysts are shown in Fig. 2C.

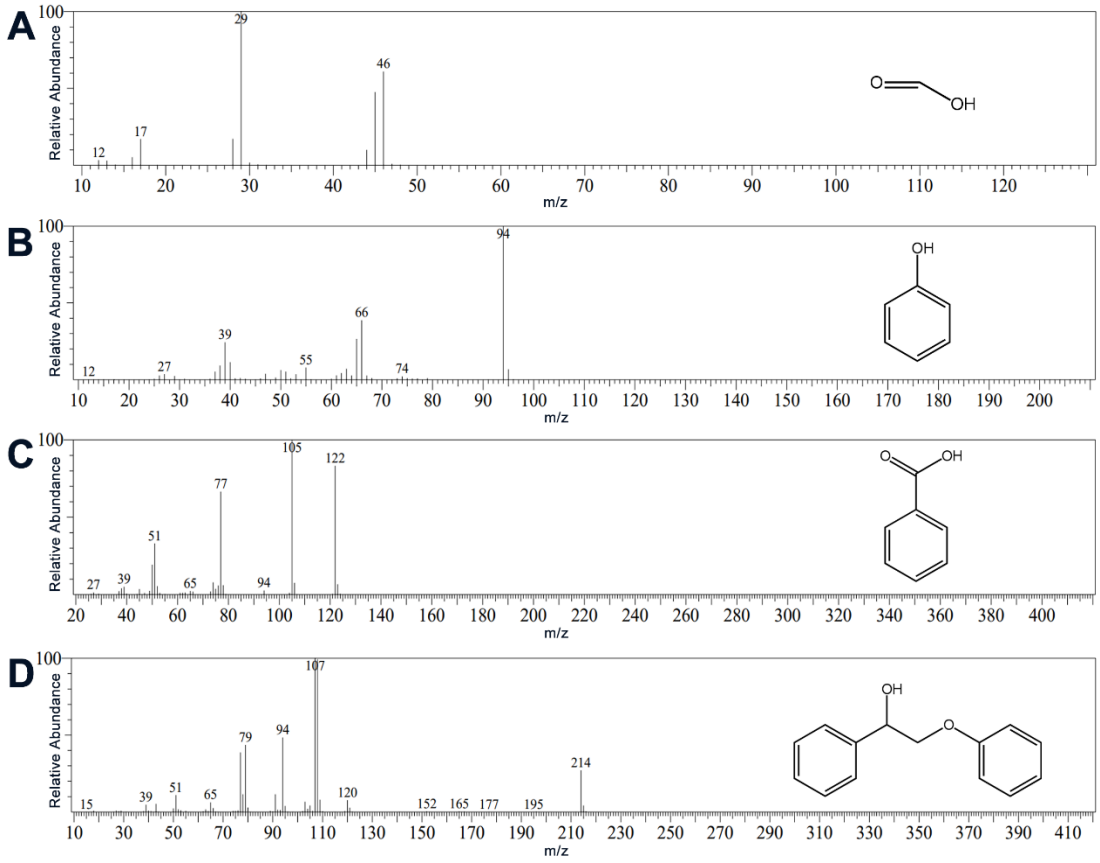

Fig. S7 Mass spectra of the electrolyte after eLDP catalysis measured by GC-MS. (A) Formate, (B) phenol, (C) benzoic acid, (D) 2-phenoxy-1-phenylethanol. Catalyst: $FeCoNi(OH)_x$@NF; applied potential: 1.5 V vs. RHE.

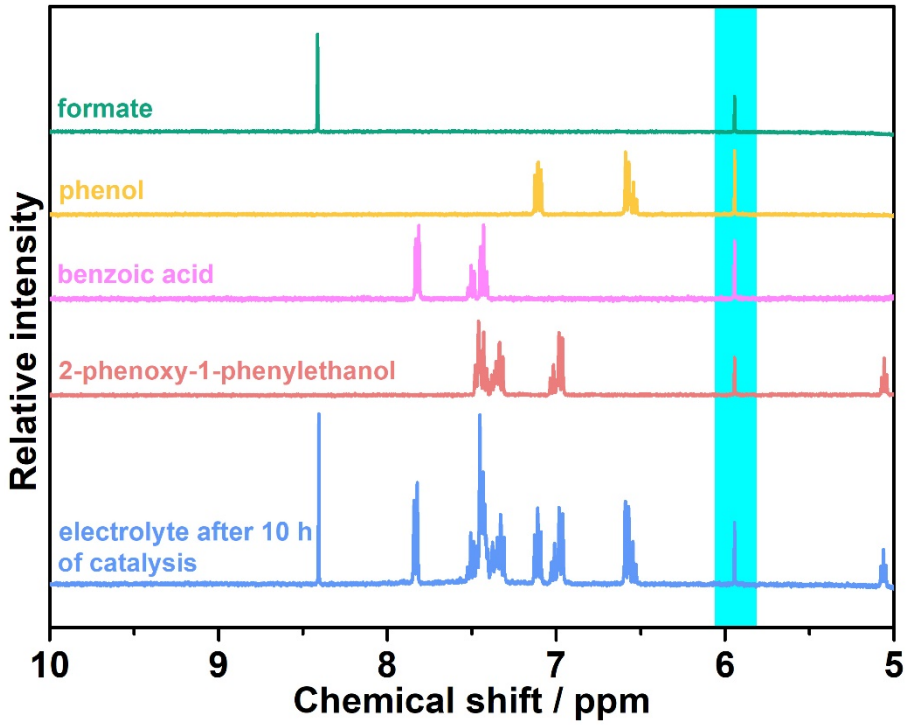

Fig. S8 ^{1}H NMR spectra of the electrolyte after eLDP catalysis and the standard spectra of 2-phenoxy-1-phenylethanol, benzoic acid, phenol and formate. The signal of the internal standard (maleic acid) is highlighted in blue. Catalyst: $FeCoNi(OH)_x$@NF; applied potential: 1.5 V vs. RHE.

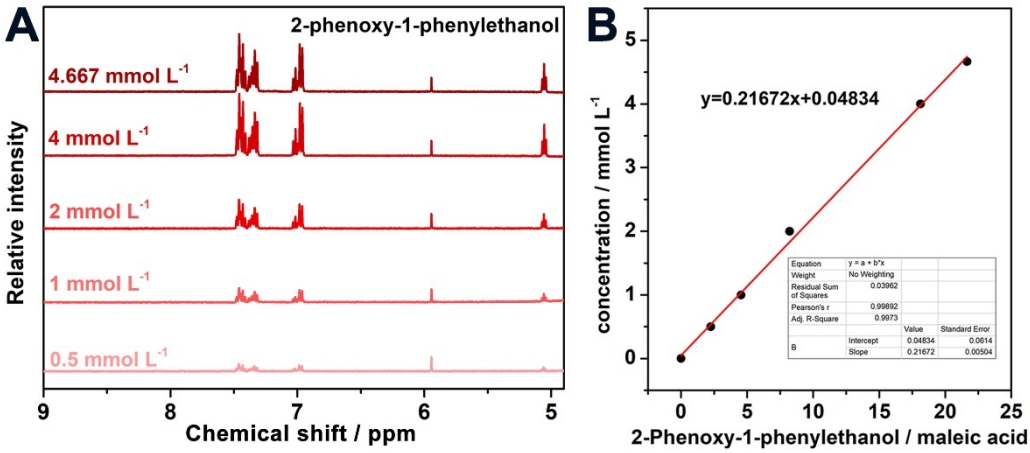

Fig. S9 (A) ^{1}H NMR spectra of 2-phenoxy-1-phenylethanol solution with standard concentration. 2-phenoxy-1-phenylethanol is dissolved in a mixed solution of MeCN and H_2O (V_{MeCN}:V_{H2O} = 1:4) with 0.5 M KOH. (B) Standard curve of 2-phenoxy-1-phenylethanol.

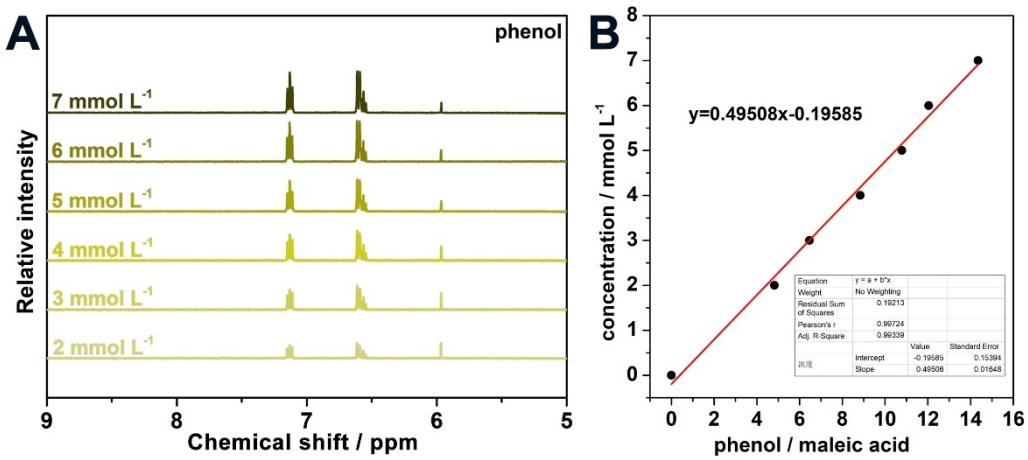

Fig. S10 (A) ^{1}H NMR spectra of phenol solution with standard concentration. Phenol is dissolved in a mixed solution of MeCN and H_2O (V_{MeCN}:V_{H2O} = 1:4) with 0.5 M KOH. (B) Standard curve of phenol.

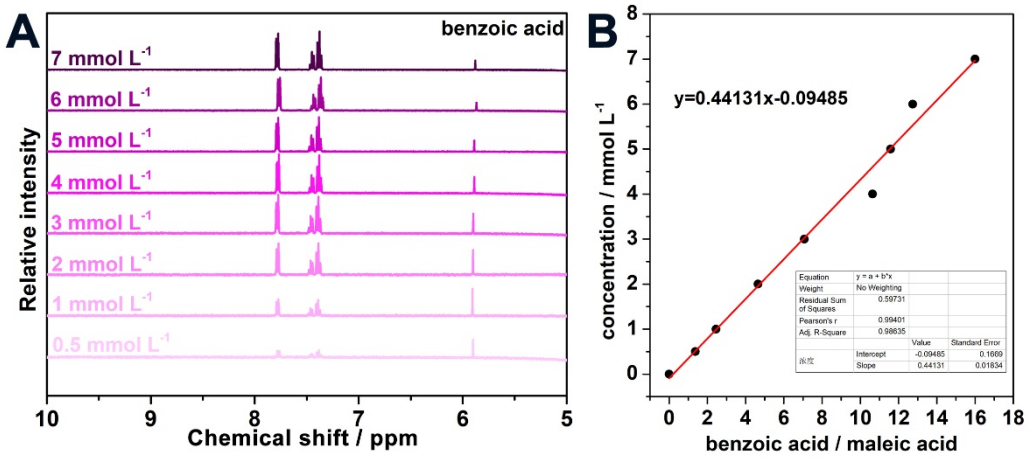

Fig. S11 (A) ^{1}H NMR spectra of benzoic acid solution with standard concentration. Benzoic acid is dissolved in a mixed solution of MeCN and H_2O (V_{MeCN}:V_{H2O} = 1:4) with 0.5 M KOH. (B) Standard curve of benzoic acid.

Table N1. Comparison of eLDP performance. All the listed measurements were conducted in air at room temperature.

Catalysts	Dosage of catalyst	Type of lignin model	Electrolyte	Electrolysis conditions	Conv. (%)	FE (%)	Ref.
$FeCoNi(OH)_x$@NF	0.5*0.5 cm	1 g L^{-1} 2-phenoxy-1-phenylethanol	V_{MeCN}:V_{H2O}=1:4, c_{KOH}=0.5 M	1.42 V vs. RHE, 5 h	51.5	35.9	This work
Pt sheet	20*20*0.1 mm	0.025 M 2-phenoxy-1-phenylethanol	0.1 M $LiClO_4/CH_3CN$	1.61 V vs. Ag/Ag^+, 8 h	43.5	-	6
		0.025 M 2-phenoxy-acetophenone		1.71 V vs. Ag/Ag^+, 8 h	39.6		
		0.025 M 2-phenoxy-1-phenylethane		1.63 V vs. Ag/Ag^+, 8 h	43.4		
Pt foil	10*10*0.3 mm	0.2 mmol 2-phenoxy-1-phenylethanol	t-BuOOH in water (70% aq. soln., 1 mmol), 0.4 mmol nBu_4NOH (used as a 37% MeOH solution), 1 mL MeCN	20 mA, 3 h	93	12	7
Pt_1/N-CNT	0.5 mg cm^{-2}, GCE	0.1 mmol 2-phenoxy-1-phenylethanol	t-BuOOH (70% aq. soln., 0.5 mmol), 0.2 mmol nBu_4NOH (used as a 37% MeOH solution), 1 mL MeCN	20 mA, 5.0 V vs. Ag/AgCl, 5 h	99	5.6	8
Co-doped $NiOOH/MoS_2$	-	0.2 mmol 2-phenoxy-1-phenylethanol	t-BuOOH (55% aqueous solution, 1 mmol), 0.2 mmol nBu_4NOH (1.0 M MeOH solution), 10 mL MeCN	3.5 V vs. Ag/AgCl, 5 h	93	-	9
Tetraphenyl-21H,23H-porphine palladium(II)/CNT	0.5 mg, carbon paper	0.2 mmol 2-phenoxy-1-phenylethanol	t-BuOOH (70% aq. soln., 1.0 mmol), nBu_4NOH (0.4 mmol, used as 40% MeOH solution), 2 mL MeCN	15 mA, 5 h	99	-	10

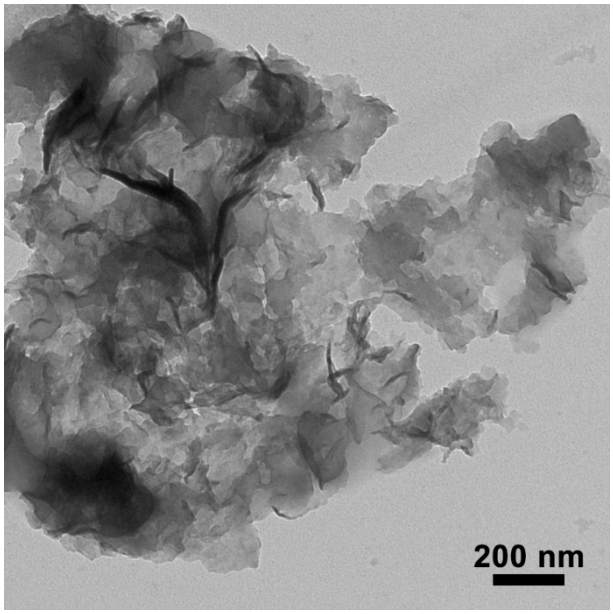

Fig. S12 TEM image of the ternary $FeCoNi(OH)_x$@NF catalyst after eight eLDP cycles.

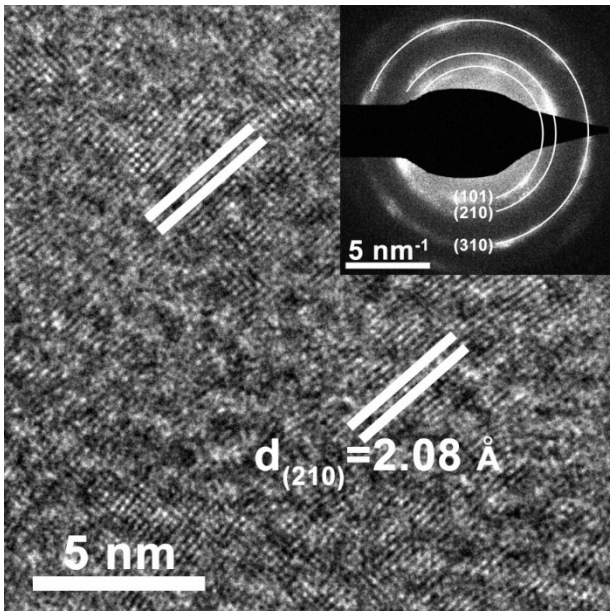

Fig. S13 HRTEM image and the SAED pattern of $FeCoNi(OH)_x$@NF after eight eLDP cycles.

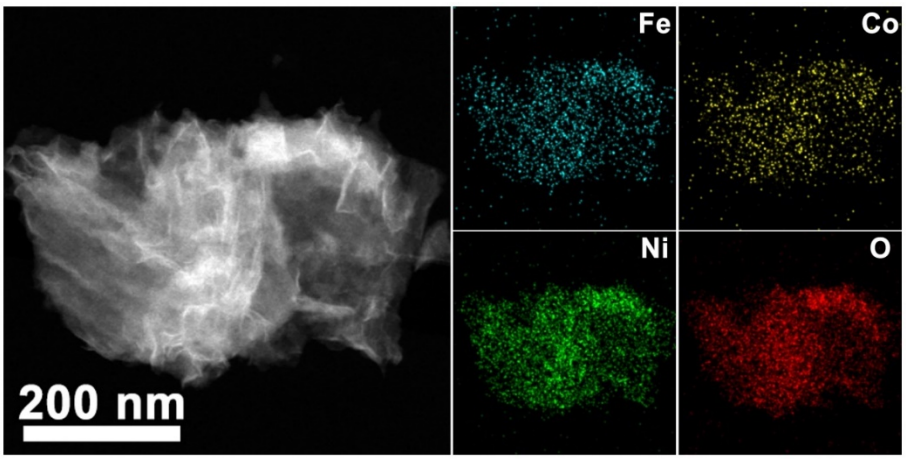

Fig. S14 HAADF-STEM image and elemental mapping of $FeCoNi(OH)_x$@NF after eight eLDP cycles.

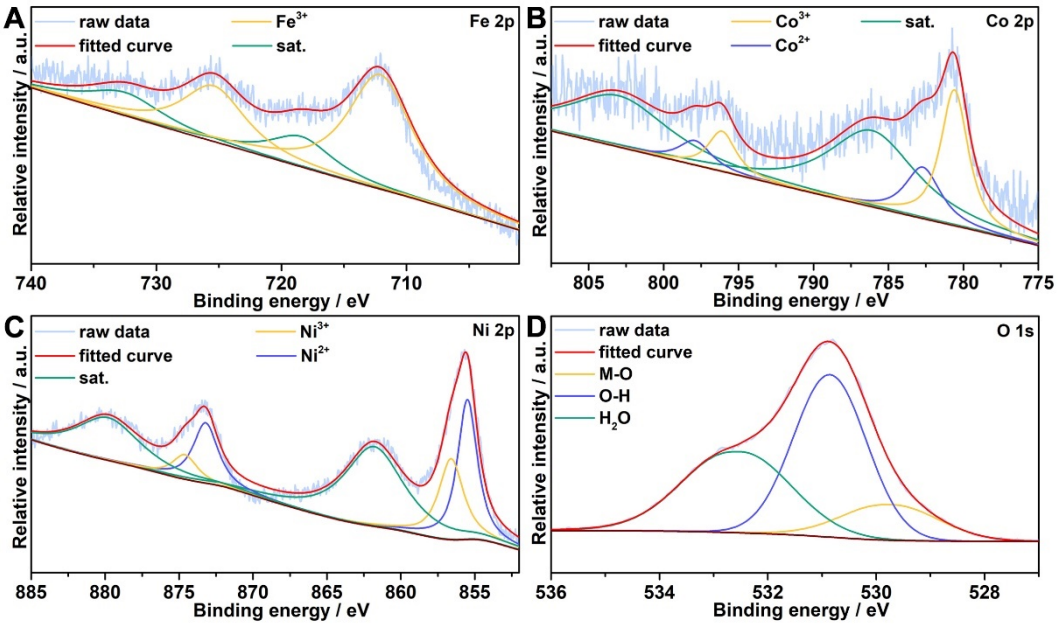

Fig. S15 (A-D) XPS spectra of Fe, Co, Ni and O of $FeCoNi(OH)_x$@NF after eight eLDP cycles.

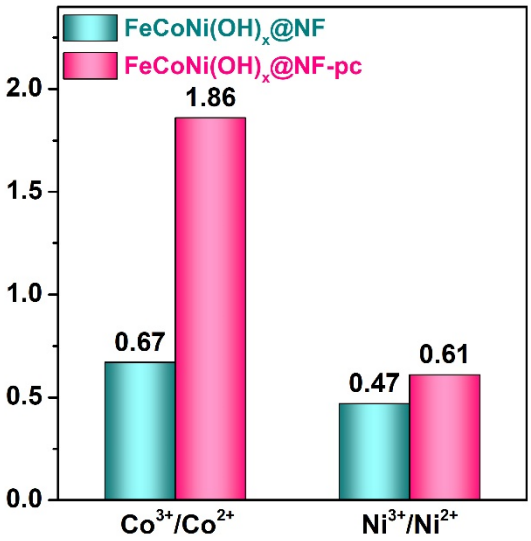

Fig. S16 Atomic ratio of Ni and Co species with specific valence before and after eight eLDP cycles.

Reference

1. C. Dong, M. Guo, W. Gao, P. Hao, F. Lei, J. Xie and B. Tang, *J. Colloid Interface Sci.*, 2022, **627**, 891-899.

2. M. Hao, J. Chen, J. Chen, K. Wang, J. Wang, F. Lei, P. Hao, X. Sun, J. Xie and B. Tang, *J. Colloid Interface Sci.*, 2023, **642**, 41-52.

3. Z. Wei, W. Sun, S. Liu, J. Qi, L. Kang, J. Li, S. Lou, J. Xie, B. Tang and Y. Xie, *Particuology*, 2021, **57**, 104-111.

4. J. Xie, X. Yang, Y. Wang, L. Kang, J. Li, Z. Wei, P. Hao, F. Lei, Q. Wang and B. Tang, *Chem. Commun.*, 2021, **57**, 11517-11520.

5. J. Xie, J. Zhang, S. Li, F. Grote, X. Zhang, H. Zhang, R. Wang, Y. Lei, B. Pan and Y. Xie, *J. Am. Chem. Soc.*, 2013, **135**, 17881-17888.

6. J. Chen, H. Yang, H. Fu, H. He, Q. Zeng and X. Li, *Phys. Chem. Chem. Phys.*, 2020, **22**, 11508-11518.

7. L. Ma, H. Zhou, X. Kong, Z. Li and H. Duan, *ACS Sustain. Chem. Eng.*, 2021, **9**, 1932-1940.

8. T. Cui, L. Ma, S. Wang, C. Ye, X. Liang, Z. Zhang, G. Meng, L. Zheng, H.-S. Hu, J. Zhang, H. Duan, D. Wang and Y. Li, *J. Am. Chem. Soc.*, 2021, **143**, 9429-9439.

9. J. Xu, J. Meng, Y. Hu, Y. Liu, Y. Lou, W. Bai, S. Dou, H. Yu and S. Wang,

Research, 2023, **6**, 0288.

10. P. Ren, L. Shi, Z. Kan, J. Bai, Y. Liu, S. Yang, S. Li and S. Liu, *Catal. Sci. Technol.*, 2024, **14**, 973-979.